BIOCHEMISTRY

 Volume 46, Number 11 March 20, 2007

Articles

Brominated Lipids Identify Lipid Binding Sites on the Surface of the Reaction Center from *Rhodobacter sphaeroides*†

Aleksander W. Roszak,‡ Alastair T. Gardiner,§ Neil W. Isaacs,*,‡ and Richard J. Cogdell*,§

Department of Chemistry, WestCHEM, and Division of Biochemistry and Molecular Biology, IBLS, Glasgow Biomedical Research Centre, University of Glasgow, 120 University Place, Glasgow G12 8TA, U.K.

Received October 16, 2006; Revised Manuscript Received December 18, 2006

ABSTRACT: This study describes the use of brominated phospholipids to distinguish between lipid and detergent binding sites on the surface of a typical α-helical membrane protein. Reaction centers isolated from *Rhodobacter sphaeroides* were cocrystallized with added brominated phospholipids. X-ray structural analysis of these crystals has revealed the presence of two lipid binding sites from the characteristic strong X-ray scattering from the bromine atoms. These results demonstrate the usefulness of this approach to mapping lipid binding sites at the surface of membrane proteins.

As more X-ray crystal structures of integral membrane proteins become available, attention is being focused on the ways in which these proteins interact with the bilayer lipids. Sometimes, when these lipids are bound either within the interior of the protein complex, e.g., as integral cofactors in photosystem I (PSI)[1] (*1*), or between protein subunits as in cytochrome bc_1 (*2*), the complete lipid structure can be resolved. On other occasions, crystal structures of membrane protein complexes reveal surface-exposed nonprotein electron density that can be unambiguously interpreted as specific lipids (*3*) since the electron density contains clear features that can be interpreted as specific lipidic head groups or, in the case of phospholipids, density for the phosphate group. A cardiolipin (CDL) molecule, fitted into electron density on the surface of the reaction center (RC) from *Rhodobacter sphaeroides* (see Figure 2 in ref *3*), is a good example of a well-defined annular lipid. More often, however, the nonprotein electron density around the outer surface of the membrane protein appears as elongated stretches that could represent either fragment(s) of the hydrophobic tail(s) of a lipid, with the head group completely disordered, or a bound detergent molecule. Figure 1a illustrates this, showing part of the surface of the RC where there are several tubelike stretches of electron density. With RC structures [crystallized in the detergent *N*,*N*-dimethyldodecylamine *N*-oxide (LDAO)], such densities are usually assigned to LDAO molecules, but parallel, pairwise arrangements of these stretches suggest that these LDAO molecules are actually located in lipid binding sites on the RC hydrophobic surface or indeed could represent two lipid fatty acid tails where the head group is disordered.

† This research was performed as part of the Membrane Protein Structure Initiative, funded by the Biotechnology and Biological Sciences Research Council. A.T.G. is supported by EU FP6 Integrated Project E-MeP.

* To whom correspondence should be addressed. N.W.I.: telephone, +44-141-3305954; fax, +44-141-3303779; e-mail, n.isaacs@chem.gla.ac.uk. R.J.C.: telephone, +44-141-3304232; fax, +44-141-3303779; e-mail, r.cogdell@bio.gla.ac.uk.

‡ Department of Chemistry, WestCHEM.

§ Division of Biochemistry and Molecular Biology, IBLS.

[1] Abbreviations: PSI, photosystem I; RC, reaction center; LDAO, *N*,*N*-dimethyldodecylamine *N*-oxide; Bchl, bacteriochlorophyll; Bpheo, bacteriopheophytin; UQ_A, ubiquinone A; UQ_B, ubiquinone B; CDL, cardiolipin; PC, phosphatidylcholine; PG, phosphatidylglycerol; PE, phosphatidylethanolamine; PS, phosphatidylserine.

10.1021/bi062154i CCC: $37.00
Published on Web 02/23/2007

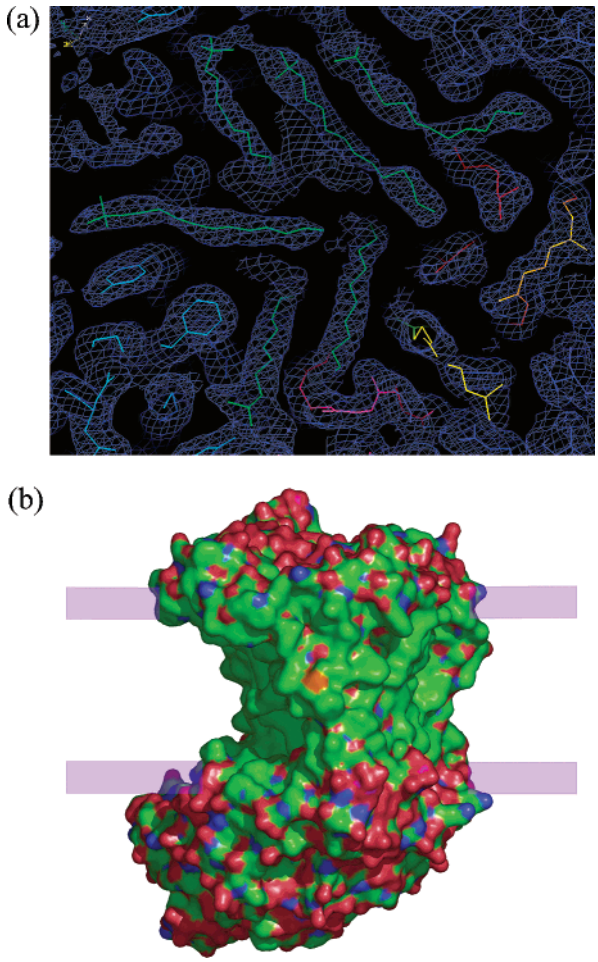

FIGURE 1: (a) LDAO molecules (green) fitted into surface $2F_o - F_c$ electron densities shown at the 0.5σ level at groove A for the 1.95 Å structure of the RC Zn mutant from *Rb. sphaeroides* (unpublished). The whole displayed area is within the transmembrane region of the RC; UQ_A is colored yellow. (b) Reaction center surface with water molecules included. C atoms are colored green, O atoms red, N atoms blue, and S atoms orange, and the approximate position of the membrane is indicated by the horizontal parallel lines.

Understanding the details of protein−lipid interactions at the surface of membrane proteins is important for two major reasons (*4*−*6*). First, many membrane proteins have a very uneven surface (see Figure 1b), yet they have to be inserted into their host membrane in such a way that the membrane remains electrically sealed, without leakage of ions across the membrane around the surface of the inserted membrane protein. There is, therefore, an important role for annular lipids that are able to mold themselves into the contours of membrane proteins ensuring that the effective surface is smoothed out and preventing local disruption of the seal. The interactions between the annular lipids and the membrane protein must also be sufficiently flexible to allow the movements and conformational changes that some membrane proteins have to undergo during their catalytic cycles (*7*, *8*). Again this flexibility must allow these motions to occur without adventitious ionic leakage. Second, specific phospholipids are often required for functional activity; e.g., CDL is essential for bovine heart cytochrome *c* oxidase (*9*), the mitochrondrial ADP/ATP carrier (*10*), and cytochrome bc_1 (*2*).

Purification and crystallization of membrane proteins require detergent solubilization, a process that usually removes the vast majority of annular lipids. In some cases, it can be beneficial to augment the purified lipid-depleted membrane protein complex with lipids prior to crystallization to produce better diffracting crystals (*11*, *12*). In at least one case, retention of the native lipids in the crystallization drop, by avoiding solubilization of the protein, has also led to significant improvement in crystal quality (*13*). Usually, however, any lipids remaining at the protein surface after solubilization are not sufficiently ordered to be easily detected and modeled in residual electron density maps. If the annular lipids have been completely stripped off the protein, then the putative lipid binding sites may be filled instead with detergent molecules, some of which may be ordered.

This paper describes a general method that uses heavy-atom derivatives of membrane lipids to unequivocally identify annular lipid binding sites on the surface of a membrane protein. By including heavy atoms, e.g., bromines, in the hydrophobic tail(s) of lipids and adding these lipids during the crystallization of the membrane protein, we are able to use X-ray crystallography to locate the heavy atoms and, therefore, positively identify that electron density as being due to lipids.

To test if this approach is feasible, easily crystallizable RCs from the purple photosynthetic bacterium *Rb. sphaeroides* strain R26-1 were used as a model membrane protein (*14*, *15*). The structure of this RC is well-characterized and has been described in a number of reviews (*16*−*19*). Brominated lipid derivatives are easily produced, provided the starting lipid contains at least one double bond. Bromine readily adds across double bonds in the lipid acyl chain to yield the brominated derivatives. The RC is then crystallized in the presence of the brominated lipid, and if the tagged lipid binds in an ordered manner to a site on the RC, the characteristic features of electron density can subsequently identify it. The implicit assumption that the presence of two bromine atoms does not adversely affect the affinity of the lipid at the binding sites will require further tests. This paper describes the successful use of this method in identifying two lipid binding sites on the RC surface. The lipids are defined in Experimental Procedures.

EXPERIMENTAL PROCEDURES

RC Purification and Crystallization. R26-1 RCs from *Rb. sphaeroides* were isolated and purified in the presence of the detergent LDAO as previously described (*20*). Large trigonal crystals (~0.5 mm) were grown by the vapor diffusion method using potassium phosphate as a precipitant (*21*). These crystals belong to space group $P3_121$ with one RC complex in the asymmetric unit.

Preparation and Reconstitution of Brominated Lipid into Reaction Centers. The chemical structures of all brominated lipids used in this study are shown in Figure 2. The first two, the brominated PC derivatives (dibromo-PC, **I**) 1-palmitoyl-2-stearoyl(6,7-dibromo)-*sn*-glycero-3-phosphocholine and (tetrabromo-PC, **II**) 1,2-distearoyl(9,10-dibromo)-*sn*-glycero-3-phosphocholine, in chloroform, were purchased from Avanti Polar Lipids.

Brominated phosphatidylglycerol (dibromo-PG, **III**), brominated phosphatidylethanolamine (dibromo-PE, **IV**), and

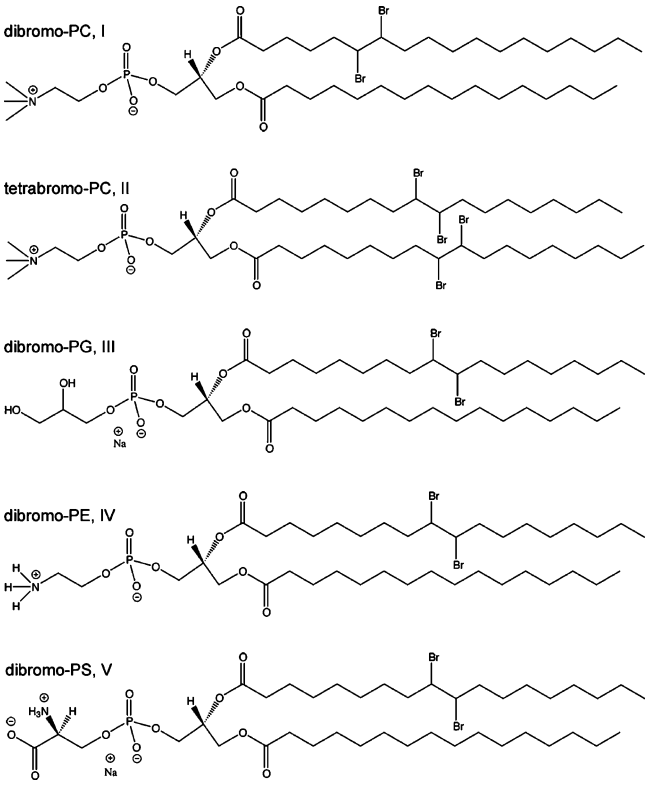

FIGURE 2: Chemical structures of brominated lipids **I**−**V** used in this study.

brominated phosphatidylserine (dibromo-PS, **V**) were synthesized from the following base compounds also purchased from Avanti Polar Lipids: PG, 1-palmitoyl-2-oleoyl-*sn*-glycero-3-[phospho-*rac*-(1-glycerol)] (sodium salt); PE, 1-palmitoyl-2-oleoyl-*sn*-glycero-3-phosphoethanolamine; and PS, 1-palmitoyl-2-oleoyl-*sn*-glycero-3-(phospho-L-serine) (sodium salt).

All these base phospholipids contain a single, unsaturated double bond in the oleoyl fatty acid at positions 9 and 10. Dibromine was titrated into each lipid/chloroform mixture (20 mg/mL) until the solution retained a faint yellow color. Excess bromine was removed by flushing this solution with nitrogen and redissolving the lipid with choloroform several times. The sample was left overnight in a desiccator to remove any last traces of excess bromine. Mass spectroscopy analyses (total mass) showed that the addition of bromine across the double bond of the lipid acyl chain was essentially 100% complete with no significant side reactions (data not shown).

The brominated lipids were resuspended in 20 mM Tris, 0.1% LDAO, and 180 mM NaCl (pH 8.0), equivalent to a 1:1 (molar ratio) Br-lipid:LDAO ratio. Prior to the reconstitution, RCs were concentrated by centrifugation to a minimal volume using a 50 kDa cutoff Centricon and washed once with 20 mM Tris (pH 8.0). Two milliliters of the Br-lipid solution was added to the Centricon, sealed, and incubated at 4 °C overnight. The sample was then concentrated to an OD_{800} of 70 and crystallized as described above.

X-ray Diffraction Data Collection, Processing, and Structure Refinement. The data processing and final structure refinement statistics for six structures together with their Protein Data Bank entries are listed in Table 1. Samples of different RC crystals were all gradually equilibrated in mother liquors containing increasing concentrations of ethylene glycol (5−30%, v/v) before being looped and quickly placed in a stream of N_2 at 100 K. Data sets, for complexes denoted **I-A** and **II**, were collected using X-rays with a wavelength of 0.87 Å, far from the bromine absorption edge. In an attempt to increase the anomalous signal, the data sets for complexes **I-B**, **III**, **IV**, and **V** were collected at or near the bromine absorption edge using the X-rays with a λ of ca. 0.92 Å. However, these experiments did not improve the anomalous signal, due probably to radiation damage. Reducing exposure times did not improve this situation.

The data were indexed, integrated, and scaled using the HKL or HKL2000 suites of programs (*22*). All data were phased by molecular replacement with AMoRe (*23*) using a 1.95 Å resolution structure of the RC Zn mutant from *Rb. sphaeroides* (unpublished data) as an initial model. Further computations were carried out using programs from the CCP4 package (*24*). All refinements used a maximum likelihood method as implemented in REFMAC (*25*) with the use of the TLS thermal mode of refinement which allows a separation of the overall lattice vibrations before the standard restrained refinement of atomic coordinates and the individual atom isotropic *B*-factors (*26*). The whole asymmetric unit containing one RC complex was assigned as a single TLS group in the structures reported here. The TLS refinement and the presence of very low-resolution reflections in our data sets led to more clear RC surface features in the electron density maps. Manual rebuilding of the RC protein chains and fitting of molecules of phospholipids, LDAO, glycerol, and phosphate ions into the surface electron densities were carried out using QUANTA (Accelrys) and COOT (*27*). REFMAC dictionaries for all phospholipids were created using the Dundee PRODRG server (*28*). Occupancies of the surface molecules were adjusted manually to approximately equalize their atomic *B*-factors to the overall Wilson plot *B*-factor and to the *B*-factors of the adjacent protein atoms. For the brominated lipids, the occupancies were estimated using anomalous difference data as described below. The occupancies were not refined. During the refinement, the models were monitored for geometrical quality using PROCHECK (*29*) and the validation features of COOT (*27*). Figures were prepared using QUANTA (Accelrys), COOT (*27*), and PyMOL (*30*).

RESULTS

Transmembrane Hydrophobic Portion of the Surface of the Reaction Center. The three-dimensional structure of the RC from *Rb. sphaeroides* has a pseudo-2-fold symmetry between the L and M protein chains, and their 10 transmembrane helices form an S shape cross section in projection at the level of the membrane (for reference, see Figure 4a of ref *31*). This arrangement produces two symmetrically related major grooves in the hydrophobic surface of RC, one of them associated with the tail of ubiquinone A (UQ_A) and another with the tail of ubiquinone B (UQ_B). These two grooves are not exactly similar in shape due to the symmetry breaking presence of the single transmembrane helix of protein H. This helix is located on the edge of the groove associated with UQ_A and makes this groove deeper than the groove associated with UQ_B; it also produces a smaller groove that is occupied by the molecule of CDL. However, the difference between two major grooves is not only in

Table 1: Data Collection and Refinement Statistics (all structures in space group $P3_121$)

	dibromo-PC (**I-A**)[a]	tetrabromo-PC (**II**)[a]	dibromo-PC (**I-B**)[a]	dibromo-PG (**III**)[a]	dibromo-PE (**IV**)[a]	dibromo-PS (**V**)[a]
Protein Data Bank entry	2HG3	2HG9	2HH1	2HHK	2HIT	2HJ6
resolution range (Å)	34.36−2.70	39.36−2.45	46.03−2.55	46.03−2.50	46.03−2.75	39.28−3.00
outer shell (Å)	2.85−2.70	2.58−2.45	2.69−2.55	2.64−2.50	2.90−2.75	3.16−3.00
beamline	9.6 at SRS	9.6 at SRS	BM14 at ESRF	BM14 at ESRF	BM14 at ESRF	10.1 at SRS
CCD detector	ADSC Quantum4	ADSC Quantum4	Marmosaic225	Marmosaic225	Marmosaic225	Marmosaic225
wavelength (Å)	0.87000	0.87000	0.91929	0.91920	0.91929	0.92000
cell dimensions (Å)						
$a = b$	139.84	139.55	139.54	139.42	139.29	139.35
c	184.34	184.61	183.96	183.70	183.84	183.22
no. of unique reflections	57840	76588	67857	71485	54102	41533
redundancy (outer shell)[b]	5.8 (5.8)	8.6 (7.8)	15.9 (16.1)	10.9 (11.0)	10.9 (11.1)	6.9 (7.0)
completeness (%)	99.9 (100.0)	99.7 (100.0)	100.0 (100.0)	99.6 (99.4)	99.9 (100.0)	99.7 (100.0)
mean I/σ	14.6 (2.6)	18.0 (3.8)	22.6 (5.8)	22.8 (4.6)	23.0 (4.3)	15.3 (3.1)
R_{merge}[c] (%)	8.2 (62.9)	6.8 (61.4)	8.8 (53.8)	5.9 (54.3)	6.6 (56.9)	8.5 (57.5)
R_{pim}[d] (%)	4.1 (31.7)	2.4 (23.2)	2.4 (14.2)	2.0 (17.8)	2.2 (18.6)	3.7 (24.9)
refinement R factor[e] (%)	16.4	17.9	17.8	17.2	18.2	17.4
R_{free}[e] (%)	19.9	20.9	21.0	19.7	22.2	22.7
Ramachandran plot features[f] (%)	91.8/7.9/0.0	92.4/7.3/0.0	92.1/7.6/0.0	92.7/7.0/0.0	91.1/8.6/0.0	91.0/8.7/0.0
rmsd						
bond lengths (Å)	0.019	0.019	0.019	0.019	0.019	0.018
bond angles (deg)	1.86	1.74	1.76	1.76	1.88	1.94
coordinate error[g] (Å)	0.265/0.136	0.198/0.115	0.227/0.108	0.203/0.104	0.319/0.152	0.502/0.192
no. of non-H atoms used in refinement	7921	7843	7923	7824	7852	7685
mean atomic/Wilson plot B factor (Å^2)	53.5/57.8	55.5/51.5	52.6/54.2	64.8/59.6	70.0/74.5	70.2/81.1

[a] The lipid formula is shown in Experimental Procedures. [b] Values in parentheses are for the highest-resolution shell. [c] $R_{merge} = \sum_{hkl}\sum_i|I_i(hkl) - \langle I(hkl)\rangle|/\sum_{hkl}\sum_i I_i(hkl)$. [d] Precision indicating merging R factor. $R_{pim} = \sum_{hkl}[1/(N-1)]^{1/2}\sum_i|I_i(hkl) - \langle I(hkl)\rangle|/\sum_{hkl}\sum_i I_i(hkl)$ (*36*, *37*), where N is the redundancy for the hkl reflection, calculated by SCALA from the CCP4 suite (*24*). [e] $R = \sum_{hkl}||F_o(hkl)| - |F_c(hkl)||/\sum_{hkl}|F_o(hkl)|$ for all data except for 5% that was used for the R_{free} calculations. [f] Percentages of residues in most favored/additionally allowed/disallowed regions. [g] Estimated standard uncertainty; the first value was calculated using the method of Cruickshank (*38*) and second one based on maximum likelihood as implemented in REFMAC (*25*).

shape. They also differ significantly in their molecular order. In the groove associated with UQ_A, the phytol tails of pigments forming the active branch [Bchl B302, Bchl B304, and Bpheo P402 (PDB file labeling)] and the isoprenoid tail of UQ_A are all well ordered. On the other hand, in the groove associated with UQ_B, the phytol tails of Bchl B301 and Bpheo P401, and the tail of UQ_B are all less well ordered. UQ_B, when it is fully reduced, has to leave the RC and deliver its reducing equivalents to the cyclic electron transfer pathway (*32*). It is not surprising, therefore, that this portion of the surface area of the RC through which UQ_B has to move is less rigid.

Differentiation between Brominated Lipid and Detergent. Figure 3 presents an example of the residual $F_o - F_c$ electron density on the surface of the RC cocrystallized with the brominated phosphatidylcholine (dibromo-PC, **I**), which is significantly different than the tubular densities shown in Figure 1a. This density shows two protruding features, consistent with the more pronounced scattering of X-rays from the heavier bromine atoms. These features allow the fitting of the respective brominated lipid used for cocrystallisation with the RC.

Using the data from experiment **I-A**, it has been possible to locate the positions of dibromo-PC at two sites on the surface of the RC where density had been previously assigned to LDAO molecules. These two positions are labeled sites A and B, as the lipids are found to be in close contact with the isoprenoid tails of UQ_A and UQ_B, respectively. Interestingly, association of tightly bound phospholipids with quinones Q_A and Q_B was also observed in the

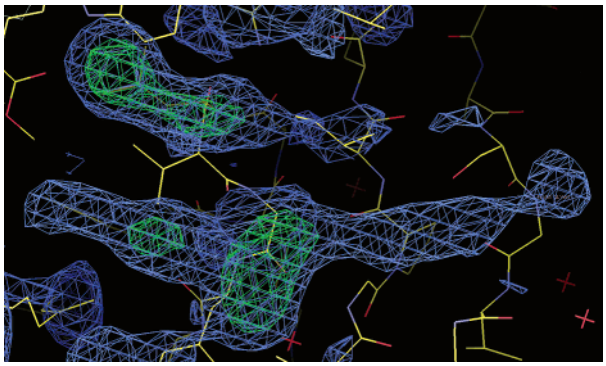

FIGURE 3: Example of the RC surface $F_o - F_c$ electron density after molecular replacement and before the fit of the lipid (for structure **I-B**; blue contour drawn at the 2.3σ level and the green contour at the 4.5σ level). The RC protein is represented as a yellow stick-style model.

structures of cytochrome b_6f (*33*) and the reaction center of PSI (*1*).

Fourier maps computed with the anomalous differences as coefficients confirmed the positions of the bromine atoms. The heights of the bromine peaks in these maps were compared with that of the anomalous peak for the iron atom, always present at 100% occupancy, in the RC. These comparisons, together with the values of the imaginary scattering factors ($\delta f''$) for Br and Fe atoms at the wavelengths of the X-rays that were used, allowed an estimation of the occupancy of Br atoms and, therefore, of the bound, ordered brominated lipids. This was found to be ~15−25%. However, higher electron density was observed in the

residual $F_o - F_c$ maps for the aliphatic portions of the lipids, and in particular for the brominated stearoyl fatty acid tail. On the basis of the analysis of the temperature factors, the phospholipid molecules were therefore refined with occupancies fixed at 50% and the bromine atoms with occupancies fixed at 12−25% depending on the experiment. The difference in occupancies could be due to three factors. First, some RCs in the crystal could have LDAO molecules bound in these sites, which would then be counted as putative fatty acid tails. Second, some of RCs could retain original membrane lipids bound in these sites. Finally, some of the Br atoms may have been removed due to X-ray-induced cleavage of C−Br bonds.

Brominated Lipids at Site A. Figure 4a shows a surface view of a RC. The smaller groove on the left-hand side of helix H is filled with the CDL, which resists the solubilization process and is found at this site (for convenience termed site C) in most of our RC structures (*3*, *15*). The second, larger groove on the right-hand side of helix H is typically occupied, in the absence of added brominated phospholipids, with the elongated tubelike stretches of electron density that can be fitted only reasonably with LDAO detergent molecules (Figure 1a). However, as shown in panels a and b of Figure 4, when the RC has been cocrystallized with brominated lipid I, the lipid binds in the deep crevice between helix H and the tail of UQ_A. Several ordered detergent molecules (represented as stick models) shown near the lipid site may also indicate less tight lipid binding sites that are, however, not filled with the brominated lipids in this structure.

Figure 5a shows lipid I with its electron density after the final structure refinement. The higher electron densities for the Br atoms and the phosphate group are evident. The two fatty acid tails of this lipid coincide in space and orientation with the two LDAO molecules previously fitted in this site (Figure 5b) in RCs crystallized without added lipids.

Details of Lipid−Protein Interactions in Site A. The fatty acid tails of the lipid **I** found in site A form mainly hydrophobic interactions with the surrounding, predominantly hydrophobic residues of helix H (Leu H24, Leu H27, Ile H28, Gln H32, and Phe H56) and of protein M (Phe M258 and Trp M268), with the extensive fragment (C12−C30) of the isoprenoid tail of UQ_A, and with phytol tails of Bchls B302 and B304. Of particular interest is the aromatic ring of Phe M258 that is approximately parallel to the lipid C36−C37 bond (bromine atoms are attached to these carbon atoms). In a natural lipid, this orientation at a distance of 3.5−3.6 Å would produce a very good $\pi-\pi$ stacking interaction with the C36═C37 pair. The hydrophilic portion of the lipid **I** forms several hydrogen bonds to the surrounding residues, namely, to the OH group of Tyr H40, to the carbonyl oxygen and to the side chain amide N atom of Asn H52, to the carbonyl bond of Gly M257, and to water molecule X169. Asparagine H52 forms a limiting barrier closing site A. The neighboring Arg M253 has been modeled with two alternate conformations of its side chain with equal occupancies, one of which would clash with the lipid but could form an H-bond with the head group of a bound LDAO molecule. This is probably due to the mixed occupancy of this site in the different RC molecules in the crystal.

Brominated Lipids at Site B. Electron density features similar to those found in site A identified a second binding

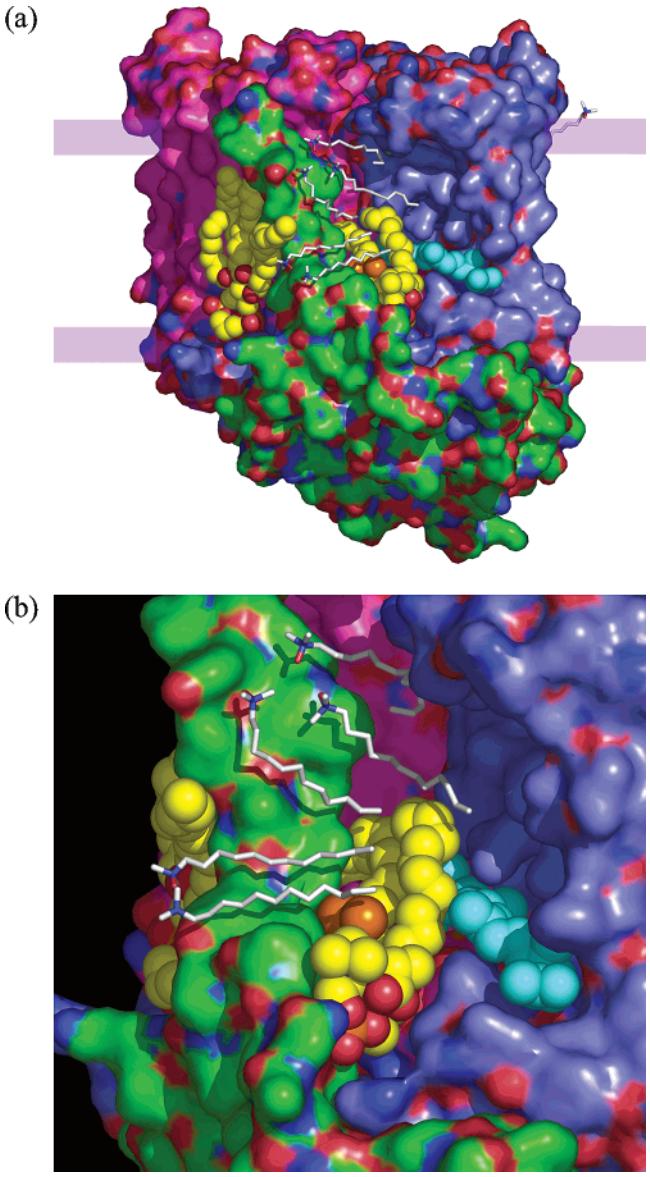

FIGURE 4: (a) Site A (in the groove to the right of helix H) and site C (in the groove to the left of helix H) containing tightly bound dibromo-PC (**I**, from structure **I-A**) and CDL molecules, respectively. The approximate position of the membrane is indicated by the horizontal parallel lines. (b) Site A with bound dibromo-PC shown in detail. The M chain (including pigments) is shown as a pink surface, the L chain (including pigments) as a blue surface, and the H chain as a green surface. The brominated lipid is represented with van der Waals spheres with C atoms colored yellow, O atoms red, and Br and P atoms orange. UQ_A is drawn as cyan spheres, and LDAO molecules are shown as white stick-style models.

site for dibromo-PC (**I**) on the opposite side of the RC complex from site A (Figure 6a). As in site A, the fatty acid tails of lipid **I** found in site B form mainly hydrophobic interactions with the surrounding protein and pigment molecules. However, the crevice, in which lipid is bound, is less deep and is not limited externally in its length. The hydrophobic "bed" for the lipid fatty acid tails of lipid **I** in site B includes various residues of protein chains M and L, the phytol tails of Bchls B301 and B303, and of Bpheo P401, and the isoprenoid tail of UQ_B. Tails of pigments B301 and P401 are rather poorly ordered, but they seem to cover the lipid tails in the binding site. The location of the dibrominated fragment of the stearoyl acyl chain is approximately above

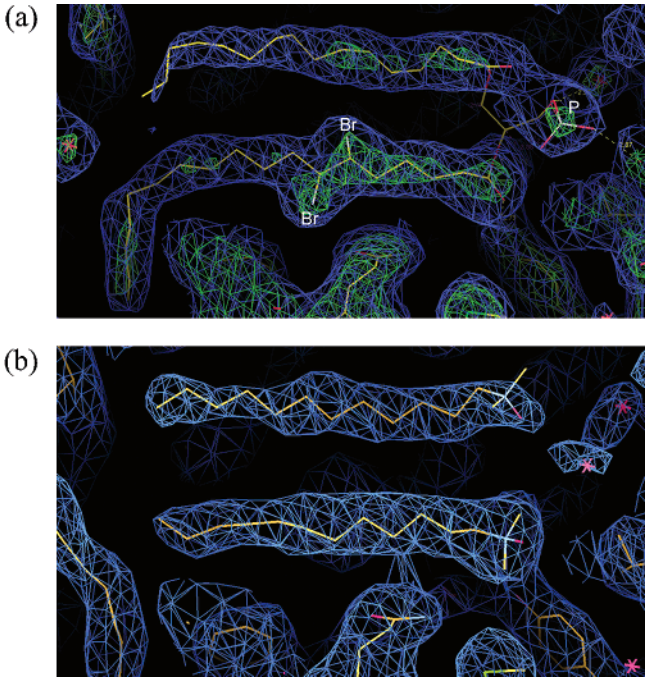

FIGURE 5: (a) $2F_o - F_c$ map for dibromo-PC (**I**, from structure **I-A**) fitted in site A. Map contours are drawn at the 2σ level in green and at the 0.5σ level of in blue. (b) Variation of Figure 1a showing LDAO molecules in site A. The $2F_o - F_c$ map contour is drawn at the 0.5σ level.

the Val 220−Tyr 222 loop of RC protein L. There is only a single H-bond binding lipid **I** in site B, and it is between the lipid phosphate group and the main chain amide NH group of Gly M31.

Cocrystallisation with Other Brominated Lipids. The cocrystallisation experiments have been repeated using brominated phospholipids **II**−**V**, and in every case, the brominated lipid could be unequivocally located in site B. Figure 6b shows site B with lipid **V**. This molecule lies next to UQ_B (both molecules are displayed using van der Waals spheres to represent the atoms). If any of the brominated lipids **II**−**V** were present in site A, they had an occupancy that was too low to be identified reliably. In these structures (despite some weak residual fragments of density observed in the region that was occupied by the lipid head group in structure **I-A**), it was only possible to fit two molecules of LDAO in site A (as in Figure 5b).

Since site B has been found to contain brominated lipid in all of our cocrystallisation experiments, it clearly does not discriminate between the 6,7-dibrominated and 9,10-dibrominated lipids. Furthermore, this site accommodates a variety of phospholipid head groups, suggesting that the dominant, stabilizing interactions in this site are the hydrophobic contacts between the acyl chains and the protein, rather than those from the specific polar head groups.

The lipids modeled in site B all show the same general structural features and lipid−protein interactions as found for lipid **I** in structure determination **I-A**. However, to accommodate the difference in the distance from the bromination site to the head group between the 9,10-brominated lipids (lipids **II**−**V**) and the 6,7-brominated one (lipid **I**), the former bind in site B with their head groups shifted farther from the hydrophobic surface of the RC; the observed difference in the position of the phosphate group due to this

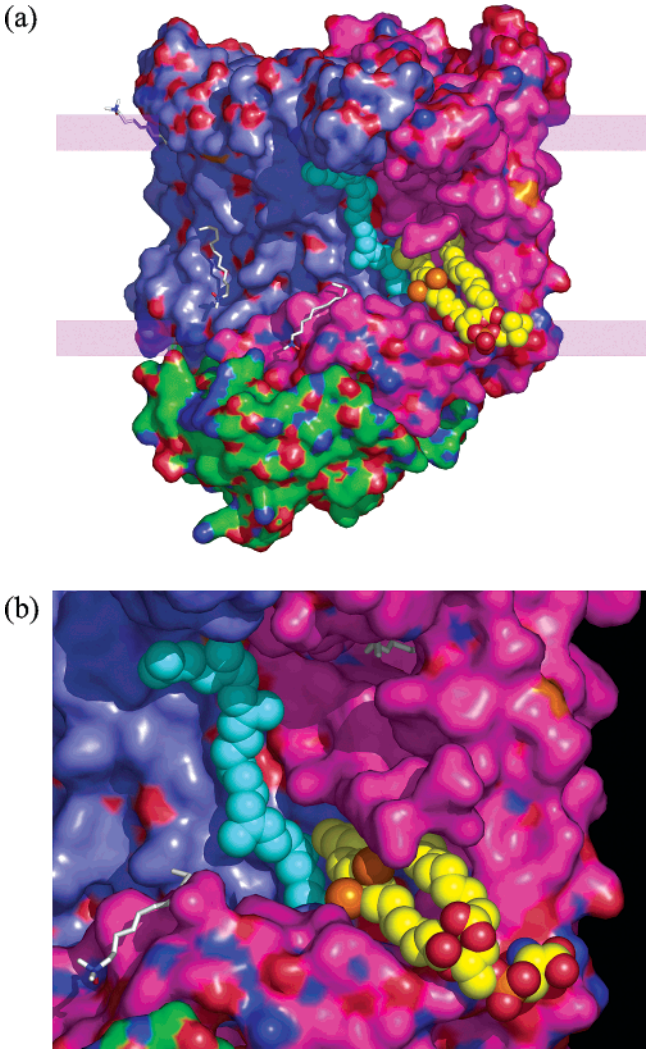

FIGURE 6: (a) Site B containing dibromo-PC (**I**, from structure **I-A**) next to UQ_B. The approximate position of the membrane is indicated by the horizontal parallel lines. (b) Site B with bound 9,10-dibromo-PS (**V**) shown in detail. The color code is that for Figure 4 with UQ_B drawn as cyan spheres.

shift is ~5 Å. This shift and the chemical differences in the head groups cause different hydrogen bond interactions. In the RC complex with lipid **III**, as well as the H-bond between the NH group of Gly M31 and the lipid phosphate group, there are two other H-bonds formed between the lipid glycerol group and the carbonyl oxygens of Arg M29 and Leu M26. In the dibromo-PE−RC complex (**IV**), the only H-bond to the Arg M29 carbonyl oxygen is formed by the ethanolamine moiety. Finally, in complex **V** (RC cocrystallized with dibromo-PS), the H-bond is formed between the Arg M29 carbonyl oxygen and the lipid phosphate group.

The binding of the added lipid can vary in different cocrystalliation trials. The structure of complex **I-B** prepared with the same dibromo-PC lipid (**I**) as complex **I-A** revealed the brominated lipid in site B only. More systematic studies aimed at investigating which factors both cause this variability and may allow higher site occupancies to be achieved are required.

Tetrabromo-PC. The structure of the RC cocrystallized with the tetrabromo-PC (lipid **II**, PC with both fatty acid tails brominated at positions 9 and 10) has similarly revealed the lipid bound in site B, but with weaker electron density

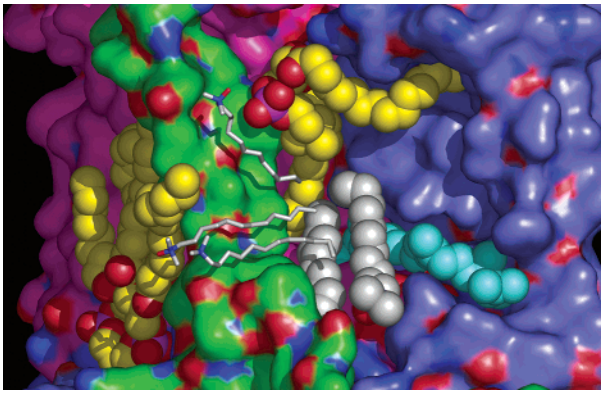

FIGURE 7: Site D (in the top portion of the groove to the right of helix H which is colored green) and site C (in the groove to the left of helix H) containing tightly bound molecules of PC and CDL, respectively (shown for structure **I-B**). The color code is that for Figure 4 with the LDAO molecules shown as white stick-style models except for two of them fitted into site A and represented with white van der Waals spheres.

for the bromine atoms, which were refined with lower occupancies (only 12%) than in the dibromo-PC case. Again, one of the fatty acid tails, the one which was bound in the same position as the dibrominated tail in complexes **I-A**, **I-B**, and **III**−**V**, was ordered while the other tail was less ordered and so more difficult to fit to the electron density. The lower occupancy of the tetrabromo-PC in site B probably reflects steric hindrance caused by the bromination of the second acyl chain.

Phospholipid in Site D. All of the RC structures described here also showed other tubular-shaped residual electron density, usually fitted as LDAO, in sites other than A or B. However, a new fourth lipid binding site, called site D, was discovered during the modeling of these residual surface features in structures **I-B** and **II**−**IV**. It is located in the groove containing UQ_A but is on the opposite side of the hydrophobic belt (Figure 7). Lipid in site D is surrounded by helices of all three protein chains, L, M, and H, and by Bchl B304. As there were no obvious "bromine" features in the electron density, a nonbrominated phospholipid has been modeled in this site, suggesting that some of the original membrane lipids bound in site D appear to have "survived" the solubilization process, just as the CDL in site C has done, though the actual identity of the lipid in site D cannot be determined from the relatively weak electron density. In structures **III** and **IV**, the head group of this lipid has been modeled with two alternative conformations. The acyl oxygen of the lipid in site D forms an H-bond with the side chain of Gln L62.

DISCUSSION

The strategy of using phospholipids tagged with bromine, as a heavy atom, has successfully enabled the unequivocal identification of lipid binding sites on the surface of our test membrane protein, the purple bacterial RC, even though the occupancy of these lipid binding sites was rather low. All of the bound lipids, brominated phospholipids in sites A and B, the CDL in site C, and the nonbrominated phospholipids in site D, adopt a "classical" position. Their head groups make polar contacts with hydrophilic residues at the interface between the hydrophilic and hydrophobic regions of the RC, and their hydrophobic, fatty acid tails extend into the hydrophobic region of the protein.

Two previous crystallographic studies with RCs from both *Thermochromatium tepidum* and *Rb. sphaeroides* (*34*, *35*) have identified lipid binding sites. A site, analogous to our site A, has been identified on the RC from purple sulfur bacterium *Tch. tepidum* where phospholipid PE is bound (*34*). Camara-Artigas et al. (*35*) reported the presence of one molecule of the glycolipid glucosylgalactosyl diacylglycerol (GGD) and one molecule of phospholipid PC on the surface of the RC from *Rb. sphaeroides*. The glycolipid GGD was found in the groove associated with UQ_A but was fitted differently than lipid **I** as determined in this study. The fatty acid chains occupy the same positions in site A as the acyl chains of lipid **I** as described above. However, the head group is positioned in the middle of the hydrophobic belt of RC. The authors (*35*) also reported a molecule of PC bound in a location coinciding in part with our site B, but with the PC orientation perpendicular to that of the brominated lipids in this site.

It is not clear what factors make it easier to bind added lipids to site B than to site A. Since lipids **II**−**VI** were not observed with significant occupancy in site A, it is possible that this site favors binding of lipids with bromination at positions 6 and 7 in contrast to bromination at positions 9 and 10. Further experiments with other types of brominated lipids at positions 6 and 7 to test this hypothesis and to investigate whether bromination at positions 9 and 10 introduces steric hindrance at site A are underway. Site A is, though, restricted in length with residue Asn H52 forming a limiting wall for the lipidic head group. As mentioned above, the aromatic ring of Phe M258 is approximately parallel to the lipid C36═C37 pair, which would produce good $\pi-\pi$ stacking interactions. This, together with the influence of Asn H52, may determine a preference in site A for 6,7-brominated lipids. Alternatively, the replacement or substitution of species bound in site A (LDAO to phospholipids during crystallization) is just much more difficult than that in site B, which is in the more flexible region of the RC surface where the diffusing quinone UQ_B is bound.

The possibility of using the anomalous signal from brominated lipids to phase X-ray diffraction data is under investigation in our laboratory. However, the relatively low occupancies of the brominated lipids need to be overcome to make this a viable phasing procedure.

ACKNOWLEDGMENT

We thank Dr. Alison Ashcroft (University of Leeds, Leeds, U.K.) for mass spectrometry analysis of lipids. The assistance of the staff of synchrotron stations 9.6 and 10.1 at SRS Daresbury (Warrington, U.K.) and of station BM14 at ESRF (Grenoble, France) is also acknowledged.

REFERENCES

1. Grotjohann, I., and Fromme, P. (2005) Structure of cyanobacterial photosystem I, *Photosynth. Res. 85*, 51−72.
2. Lange, C., Nett, J. H., Trumpower, B. L., and Hunte, C. (2001) Specific roles of protein-phospholipid interactions in the yeast cytochrome bc_1 complex structure, *EMBO J. 20*, 6591−6600.
3. McAuley, K. E., Fyfe, P. K., Ridge, J. P., Isaacs, N. W., Cogdell, R. J., and Jones, M. R. (1999) Structural details of an interaction between cardiolipin and an integral membrane protein, *Proc. Natl. Acad. Sci. U.S.A. 96*, 14706−14711.
4. Lee, A. G. (2003) Lipid-protein interactions in biological membranes: A structural perspective, *Biochim. Biophys. Acta 1612*, 1−40.

5. Lee, A. G. (2004) How lipids affect the activities of integral membrane proteins, *Biochim. Biophys. Acta 1666*, 62−87.
6. Palsdottir, H., and Hunte, C. (2004) Lipids in membrane protein structures, *Biochim. Biophys. Acta 1666*, 2−18.
7. Toyoshima, C., Nomura, H., and Tsuda, T. (2004) Lumenal gating mechanism revealed in calcium pump crystal structures with phosphate analogues, *Nature 432*, 361−368.
8. Lee, S. Y., Lee, A., Chen, J. Y., and MacKinnon, R. (2005) Structure of the KvAP voltage-dependent K^+ channel and its dependence on the lipid membrane, *Proc. Natl. Acad. Sci. U.S.A. 102*, 15441−15446.
9. Gomez, B., Jr., and Robinson, N. C. (1999) Phospholipase digestion of bound cardiolipin reversibly inactivates bovine cytochrome bc_1, *Biochemistry 38*, 9031−9038.
10. Hoffmann, B., Stockl, A., Schlame, M., Beyer, K., and Klingenberg, M. (1994) The reconstituted ADP/ATP carrier activity has an absolute requirement for cardiolipin as shown in cysteine mutants, *J. Biol. Chem. 269*, 1940−1944.
11. Zhang, H. M., Kurisu, G., Smith, J. L., and Cramer, W. A. (2003) A defined protein-detergent-lipid complex for crystallization of integral membrane proteins: The cytochrome b_6f complex of oxygenic photosynthesis, *Proc. Natl. Acad. Sci. U.S.A. 100*, 5160−5163.
12. Guan, L., Smirnova, I. N., Verner, G., Nagamori, S., and Kaback, H. R. (2006) Manipulating phospholipids for crystallization of membrane transport protein, *Proc. Natl. Acad. Sci. U.S.A. 103*, 1723−1726.
13. Sato, H., Takeda, K., Tani, K., Hino, T., Okada, T., Nakasako, M., Kamiya, N., and Kouyama, T. (1999) Specific lipid-protein interactions in a novel honeycomb lattice structure of bacteriorhodopsin, *Acta Crystallogr. D55*, 1251−1256.
14. Stowell, M. H., McPhillips, T. M., Rees, D. C., Soltis, S. M., Abresch, E., and Feher, G. (1997) Light-induced structural changes in photosynthetic reaction center: Implications for mechanism of electron-proton transfer, *Science 276*, 812−816.
15. Roszak, A. W., McKendrick, K., Gardiner, A. T., Mitchell, I. A., Isaacs, N. W., Cogdell, R. J., Hashimoto, H., and Frank, H. A. (2004) Protein Regulation of Carotenoid Binding: Gatekeeper and Locking Amino Acid Residues in Reaction Centers of *Rhodobacter sphaeroides*, *Structure 12*, 765−773.
16. Schiffer, M., and Norris, J. R. (1993) Structure and function of the photosynthetic reaction centre of *Rhodobacter sphaeroides*, in *The photosynthetic reaction center* (Deisenhofer, J., and Norris, J. R., Eds.) pp 1−12, Academic Press Inc., San Diego.
17. Lancaster, C. R., Ermler, U., and Michel, H. (1995) The structures of photosynthetic reaction centres from purple bacteria as revealed by X-ray crystallography, in *Anoxygenic Photosynthetic Bacteria* (Blankenship, R. E., Madigan, M. T., and Bauer, C. E., Eds.) pp 503−526, Kluwer Academic Publishers, Dordrecht, The Netherlands.
18. Woodbury, N. W., and Allen, J. P. (1995) The pathway, kinetics and thermodynamics of electron transfer in wild-type and mutant reaction centres of purple non-sulphur bacteria, in *Anoxygenic Photosynthetic Bacteria* (Blankenship, R. E., Madigan, M. T., and Bauer, C. E., Eds.) pp 527−557, Kluwer Academic Publishers, Dordrecht, The Netherlands.
19. Deisenhofer, J., and Michel, H. (2004) The photosynthetic reaction centre from the purple bacterium *Rhodopseudomonas viridis*, *Biosci. Rep. 24*, 323−361.
20. Farhoosh, R., Chynwat, V., Gebhard, R., Lugtenburg, J., and Frank, H. A. (1997) Triplet energy transfer between the primary donor and carotenoids in *Rhodobacter sphaeroides* R-26.1 reaction centers incorporated with spheroidene analogs having different extents of π-electron conjugation, *Photochem. Photobiol. 66*, 97−104.
21. Buchanan, S. K., Fritzsch, G., Ermler, U., and Michel, H. (1993) New crystal form of the photosynthetic reaction centre from *Rhodobacter sphaeroides* of improved diffraction quality, *J. Mol. Biol. 230*, 1311−1314.
22. Otwinowski, Z., and Minor, W. (1997) Processing of X-ray diffraction data collected in oscillation mode, *Methods Enzymol. 276*, 307−326.
23. Navaza, J. (1994) AMoRe: An automated package for molecular replacement, *Acta Crystallogr. A50*, 157−163.
24. Collaborative Computational Project Number 4 (1994) The CCP4 suite: Programs for protein crystallography, *Acta Crystallogr. D50*, 760−763.
25. Murshudov, G. N., Vagin, A. A., and Dodson, E. J. (1997) Refinement of macromolecular structures by the maximum-likelihood method, *Acta Crystallogr. D53*, 240−255.
26. Winn, M. D., Isupov, M. N., and Murshudov, G. N. (2001) Use of TLS parameters to model anisotropic displacements in macromolecular refinement, *Acta Crystallogr. D57*, 122−133.
27. Emsley, P., and Cowtan, K. (2004) Coot: Model-building tools for molecular graphics, *Acta Crystallogr. D60*, 2126−2132.
28. Schuettelkopf, A. W., and van Alten, D. M. F. (2004) PRODRG: A tool for high-throughput crystallography of protein-ligand complexes, *Acta Crystallogr. D60*, 1355−1363.
29. Laskowski, R. A. (1993) Procheck: A program to check the stereochemical quality of protein structures, *J. Appl. Crystallogr. 26*, 283−291.
30. DeLano, W. L. (2002) *The PyMOL Molecular Graphics System*, DeLano Scientific, San Carlos, CA.
31. Roszak, A. W., Howard, T. D., Southall, J., Gardiner, A. T., Law, C. J., Isaacs, N. W., and Cogdell, R. J. (2003) Crystal Structure of the RC-LH1 Core Complex from *Rhodopseudomonas palustris*, *Science 302*, 1969−1972.
32. Moser, C. C., Page, C. C., Cogdell, R. J., Barber, J., Wraight, C. A., and Dutton, P. L. (2003) Length, time, and energy scales of photosystems, *Adv. Protein Chem. 63*, 71−109.
33. Kurisu, G., Zhang, H., Smith, J. L., and Cramer, W. A. (2003) Structure of the Cytochrome b_6f Complex of Oxygenic Photosynthesis: Tuning the Cavity, *Science 302*, 1009−1014.
34. Nogi, T., Fathir, I., Kobayashi, M., Nozawa, T., and Miki, K. (2000) Crystal structures of photosynthetic reaction center and high-potential iron-sulfur protein from *Thermochromatium tepidum*: Thermostability and electron transfer, *Proc. Natl. Acad. Sci. U.S.A. 97*, 13561−13556.
35. Camara-Artigas, A., Brune, D., and Allen, J. P. (2002) Interactions between lipids and bacterial reaction centers determined by protein crystallography, *Proc. Natl. Acad. Sci. U.S.A. 99*, 11055−11060.
36. Weiss, M. S. (2001) Global indicators of X-ray data quality, *J. Appl. Crystallogr. 34*, 130−135.
37. Weiss, M. S., and Hilgenfeld, R. (1997) On the use of the merging R factor as a quality indicator for X-ray data, *J. Appl. Crystallogr. 30*, 203−205.
38. Cruickshank, D. W. J. (1999) Remarks about protein structure precision, *Acta Crystallogr. D55*, 583−601.

BI062154I